



Performance characterization of a cross-flow hydrokinetic turbine in sheared inflow



Dominic Forbush^{a,*}, Brian Polagye^a, Jim Thomson^a, Levi Kilcher^b, James Donegan^c, Jarlath McEntee^c

^a Northwest National Marine Renewable Energy Center, University of Washington, Box 352600, Seattle, WA 98195-2600, USA

^b National Renewable Energy Laboratory, 18200 CO-128, Boulder, CO 80303, USA

^c Ocean Renewable Power Company, 66 Pearl St. Suite 301, Portland, ME 04101, USA

ARTICLE INFO

Article history:

Received 2 June 2015

Revised 2 June 2016

Accepted 15 June 2016

Available online 16 June 2016

Keywords:

Performance characterization

Resource assessment

Turbulence

Cross-flow turbines

Sheared inflow

ABSTRACT

A method for constructing a non-dimensional performance curve for a cross-flow hydrokinetic turbine in sheared flow is developed for a natural river site. The river flow characteristics are quasi-steady, with negligible vertical shear, persistent lateral shear, and synoptic changes dominated by long time scales (days to weeks). Performance curves developed from inflow velocities measured at individual points (randomly sampled) yield inconclusive turbine performance characteristics because of the spatial variation in mean flow. Performance curves using temporally- and spatially-averaged inflow velocities are more conclusive. The implications of sheared inflow are considered in terms of resource assessment and turbine control.

© 2016 Elsevier Ltd. All rights reserved.

1. Introduction

Hydrokinetic energy conversion involves the extraction of kinetic energy from moving water and its conversion to electricity, analogous to the operation of wind turbines. Naturally-occurring high energy flows, such as river, tidal, or ocean currents, can be harnessed without incurring the environmental costs associated with impoundment behind a dam. Hydrokinetic energy converters are also modular and scalable [1]. This makes such systems potentially attractive to markets ranging from instrumentation (10^1 W) to small communities (10^4 W) to regional utilities (10^8 W).

Hydrokinetic turbines can be broadly categorized as axial-flow and cross-flow systems, though novel approaches are also being explored [1]. For axial-flow turbines, the axis of rotation is parallel to the flow direction, while in cross-flow turbines it is perpendicular. Cross-flow turbines may be oriented horizontally, with their axis of rotation parallel to the water surface, or vertically, with the axis perpendicular to the surface [1]. This research focuses on the performance of a horizontally-oriented cross-flow turbine. Like wind turbines, hydrokinetic turbines may be characterized by a non-dimensional power performance curve relating the performance coefficient (C_p) to the tip-speed ratio (λ), a ratio of turbine blade velocity to free-stream velocity [2]. In general, the performance curve has a global maxima corresponding to optimal conversion efficiency from kinetic to mechanical power at an associated tip-speed ratio. If the turbine's mechanical power output is known, the performance coefficient is given as

* Corresponding author.

E-mail address: forbudom@uw.edu (D. Forbush).

$$C_p = \frac{P}{\frac{1}{2}\rho AU_\infty^3} \quad (1)$$

where ρ is density of the working fluid (1000 kg/m^3 in riverine environments), A is turbine projected area (m^2), P is the mechanical power produced (W), and U_∞ is the free-stream, or inflow, velocity upstream of the turbine (m/s). Standard practice is for U_∞ to be measured close enough to the turbine to be representative of the inflow, but far enough away for axial and angular induction to be negligible [2]. C_p represents the fraction of kinetic power incident over the turbine swept area that is converted to mechanical power. The water-to-wire efficiency (η) is the product of C_p and the balance of system efficiency (e.g., generator, gearbox, power electronics). For commercial systems, electrical current and voltage output are more commonly measured than mechanical power and η may be calculated as

$$\eta = \frac{IV}{\frac{1}{2}\rho AU_\infty^3} \quad (2)$$

where I and V are the output current and voltage, respectively. The tip-speed ratio is defined as

$$\lambda = \frac{R\omega}{U_\infty} \quad (3)$$

where ω is the angular velocity of the turbine rotor (rad/s), and R is the rotor radius (m).

A challenge in riverine environments is that variations in bathymetry may give rise to horizontal or vertical shear on the same length scales as a turbine rotor [4]. Because of this, there may not be an obvious choice of U_∞ for the non-dimensional representation of performance.

This paper describes field measurements around a hydrokinetic turbine, the Ocean Renewable Power Company (ORPC) RivGen[®] turbine, on the Kvichak River near Iguigig, Alaska (USA). The turbine and the deployment site are first described, followed by a description of measurements of stream velocity. The characterization of turbine performance in the presence of strong lateral (across-rotor) shear is then presented, and the paper closes with a discussion of the implications of these results for resource characterization, turbine control, and performance assessment.

2. Background

2.1. Turbine

The RivGen turbine is a cross-flow helical hydrokinetic turbine designed to provide community-scale power (10^4 W) as an alternative to diesel generation in remote communities [5]. The turbine consists of two 4.1 m long rotors situated symmetrically about a 2.8 m wide gap housing the generator (Fig. 1).

Prior to installation, preliminary characterization was performed with tow trials in Eastport, ME. The turbine was lowered below a barge being towed at a constant velocity which resulted in near-uniform flow across the turbine. Using this method, the maximum water-to-wire efficiency was found to be $\sim 19\%$. This performance was in agreement with computational fluid dynamic simulation and is in-line with experimental performance of turbines with similar geometry [6,7].

2.2. Site description

The turbine was deployed in August 2014 on the Kvichak River just downstream of the village of Iguigig, Alaska (USA). A local coordinate system is defined in Fig. 2, with $+x$ downstream (U component of velocity), $+y$ cross-river towards the village (V component of velocity), and $+z$ upwards (W component of velocity). The origin is at the nominal center of the turbine (59.3248° N , 155.9151° W) and the rotation from an east-north-up (true) coordinate system is 107° clockwise.

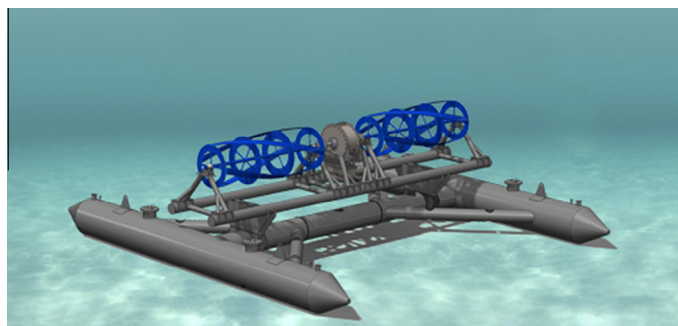


Fig. 1. Conceptual rendering of the RivGen turbine.



Fig. 2. Turbine deployment location and local coordinate system at Igiugig, AK. Satellite image from Google Earth.

3. Stream velocity characterization

3.1. Methodology

3.1.1. Measurement

Inflow velocities were measured at points upstream of the turbine from Aug 15 to 25, 2014. Measurements were made with six Nortek Aquadopp profilers (1 and 2 MHz operating frequencies) deployed in a down-looking orientation from surface catamaran platforms (Doppcats, see Fig. 3). Aquadopps sampled continuously at 1 Hz, with 0.5 m bins (bin #4 is approximately the hub-height of the turbine). The platforms were towed on tethers at 10 m spacing astern of a small skiff, which held station for 10 minutes at a variety of locations upstream of the turbine. The station-holding approach was adopted when anchors for the Doppcats were unable to hold sufficiently on the cobbled bottom. Platform locations were recorded at 5 Hz using Qstarz BT-Q1000eX GPS receivers, and this information was used to correct velocity measurements for platform motion in post-processing.

In addition, a Nortek Vector velocimeter was deployed on a sounding weight (“turbulence torpedo”) lowered from a davit at the stern of the skiff to provide turbulence measurements at higher temporal resolution (16 Hz). These velocity data are subject to contamination by platform motion which are removed using data from a synchronous Inertial Motion Unit (IMU) on-board the instrument (Microstrain 3DM-GX3-25), following [8,9]. These velocimeter measurements were made twice, each for 10 minutes, approximately 60 m upstream and starboard (+y) of the center line of the turbine at the turbine hub-height ($z = -2$ m from surface). Turbulence measurements could not be made at closer proximity without risking damage to the turbine in the event of loss of skiff propulsion.



Fig. 3. Doppcat platform for down looking Nortek Aquadopp velocity profiler (left) and sounding weight platform for Nortek Vector velocimeter (right) at Igiugig, AK.

3.1.2. Uncertainty analysis

The velocity measurements, which vary in space and time, are subject to measurement uncertainties that are dominated by the Doppler noise (ΔU_n) of the instruments. The stream-wise flow U , for example, is decomposed as

$$U(x, y, z, t) = \bar{U}(x, y, z) + U'(x, y, z, t) \pm \Delta U_n \pm \Delta U_{sk} \quad (4)$$

where \bar{U} is the mean flow calculated from 10 minutes of data, $U'(x, y, z, t)$ is an instantaneous turbulent fluctuation, and ΔU_n is estimated as a constant noise level of 0.04 m/s for the 2 MHz Aquadopps and 0.10 m/s for the 1 MHz Aquadopps (based on the “Aquapro” configuration software provided by Nortek). There are additional uncertainties resulting from imperfect station keeping, measured via GPS as $\Delta U_{sk} \approx 0.1$ m/s.

The space and time variables also have uncertainties,

$$\tilde{x} = x \pm \Delta x_{GPS} \pm \Delta x_{bs} \pm \Delta x_{sk} \quad (5)$$

which are the result of GPS errors ($\Delta x_{GPS} \approx 5$ m), beam spreading of the down looking Aquadopps ($\Delta x_{bs} \approx 3$ m), imperfect station keeping ($\Delta x_{sk} \approx 5$ m), and Doppcat clock drift ($\Delta t \approx 1$ s). These uncertainties were assumed to be uncorrelated and averaging of results significantly reduced the uncertainty, such that robust estimates of the mean flow $\bar{U}(x, y, z, t)$ at a given position are repeatable. In the analysis that follows, spatial gradients of the mean flow are only reported up to a resolution equal to the uncertainty in x .

3.1.3. Turbulence characteristics

Turbulence intensity is a simple scalar metric describing the ratio of velocity fluctuations, represented as the standard deviation, to mean velocity. Using Doppler profilers, robust estimates of the turbulence intensity TI are possible if the additional sources of variance from noise are removed [10].

$$TI(x, y, z) = \frac{\sqrt{\langle U'(x, y, z, t)^2 \rangle - \Delta U_n^2 - \Delta U_{sk}^2}}{\bar{U}(x, y, z)} \quad (6)$$

where $\langle U'(x, y, z, t)^2 \rangle$ indicates an ensemble value over 10 minutes of observations at a particular (x, y) station. The removal of noise is essential for determining the turbulence intensity from Doppler profilers, such as the Aquadopps ($\Delta U_n = 0.04$ m/s) on the Doppcat platforms. The results are verified against high-fidelity data from upstream deployments of the velocimeter ($\Delta U_n < 0.01$ m/s) on the turbulence torpedo. The velocimeter measurements also have the advantage of being well-localized in space, since they do not suffer the beam spread issue common to all profiler measurements [11].

Skewness is a measure of the asymmetry in the distribution in velocity fluctuations. Since it is a higher moment of the distribution, it can only be calculated using the low-noise velocimeter data. The skewness metric considered for each window is the adjusted Fisher–Pearson standardized moment

$$G_1 = \frac{n}{(n-1)(n-2)} \sum_{i=1}^n \left(\frac{x_i - \bar{x}}{s} \right)^3 \quad (7)$$

where n is the sample size, s the sample standard deviation, and \bar{x} the mean of the sample [12].

Turbulent kinetic energy (TKE) spectra are a measure of the energy contained at particular time scales. This is calculated using the Fast Fourier Transform (FFT) of the velocity data in 10-minute windows, which are first divided into overlapping 256 s sub-windows, detrended, and tapered. After merging every five frequency bands, the resulting spectra have 30 degrees of freedom, resulting in relatively tight confidence intervals.

3.2. Results

3.2.1. Spatial variability

The mean stream-wise flow $\bar{U}(x, y, z)$ shows a robust spatial pattern, with random turbulent fluctuations in time that are $TI \approx 10\%$ of the mean flow at most locations upstream of the turbine and in the center of the river. Fig. 4 shows gridded observations collected with the Aquadopp profilers over 10 days. The temporal and spatial variations are separated by binning individual 10-minute ensembles into 5-m resolution grid cells (using the local coordinate system) and assessing sensitivity. The spatial variations in the mean flow are extreme, and in many cases the uncertainty in measurement position is a greater source of velocity changes than the $TI \approx 10\%$ turbulence intensity at any given point.

In the following subsections, the spatial patterns addressed are cross-river y (i.e., lateral shear of inflow velocities) and depth profiles z (i.e., vertical shear of inflow velocities). For each axis investigated, the robustness of the spatial pattern is quantified with the standard error and standard deviation of the gridded mean velocity result and this is compared with velocity fluctuations expected from the average turbulence intensity TI in each grid cell.

3.2.2. Lateral shear

The lateral shear of inflow velocities across the turbine rotor (i.e., from port to starboard, y -axis) is the most striking spatial pattern. As shown in Fig. 5, the mean inflow velocity varies from 1.6 m/s at the port side of the turbine ($y = -5.5$ m) to

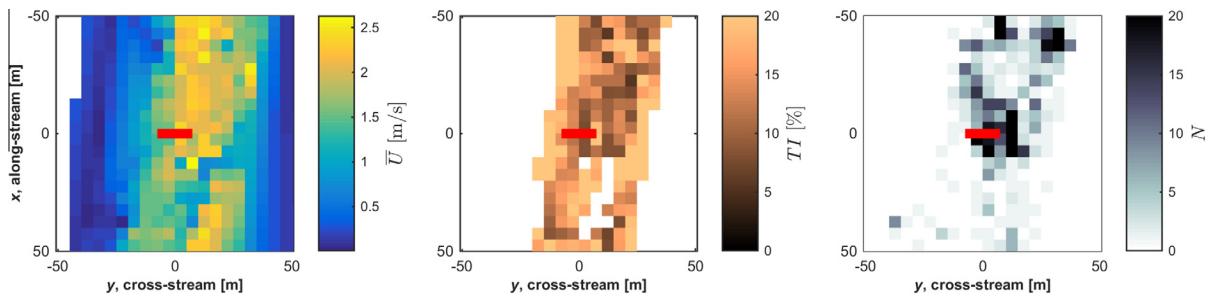


Fig. 4. All mean stream-wise flow results (left), turbulence intensities (center), and number of 10-minute averages (right) from the Doppcat station keeping measurements at the turbine hub-height, $z = -2$ m below the surface. The turbine location is shown by a thick red line at the origin. Turbulence intensity values are not shown for grid cells lacking a complete 5-minute data set ($N < 1$).

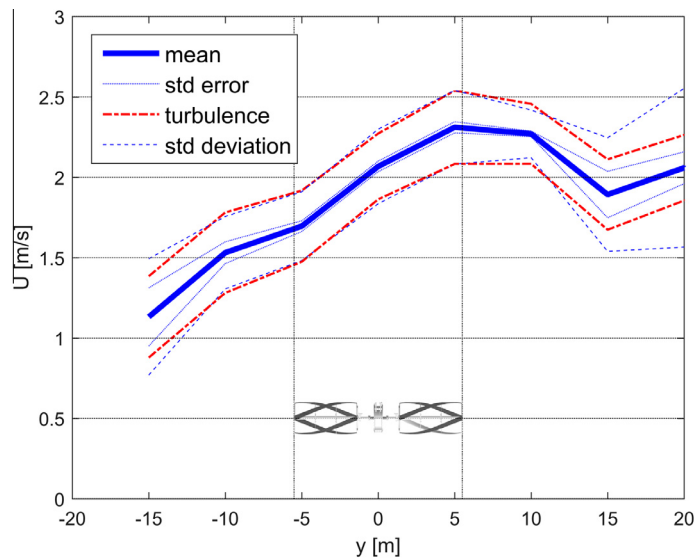


Fig. 5. Lateral shear shown as the stream-wise flow U versus cross-river dimension y . The blue dotted line is the standard error in determining the mean flow at each y . The blue dashed line is the standard deviation of individual stations. The red dashed line is variation expected from the measured turbulence intensity. The turbine is also shown ($-5.5 < y < 5.5$) m.

2.3 m/s at the starboard side of the turbine ($y = 5.5$ m). Results are the average from 338 stations lasting at least 10 minutes each, collected at positions immediately upstream of the turbine ($-20 < x < 0$ m). This 44% increase in speed is a 200% increase in the kinetic power density of the flow. This mean flow pattern is robust, as shown by the standard error lines in Fig. 5. However the individual ensembles have significant scatter, as shown by the standard deviation lines in Fig. 5. In fact, the standard deviations obtained from the uncertainties in spatial binning ($\Delta x_{\text{GPS}} \approx 5$ m) are similar, and generally exceed, the velocity fluctuations attributed to turbulence within each ensemble.

The observed shear is expected given the proximity to a river bend and the ADCP surveys completed the previous year [13]. It also appears that a turbine deployed a few meters farther east, at approximately $0 < y < 11$ m, would have experienced a more uniform inflow. Although a few meters may seem an extreme sensitivity in a river that is 150 m wide, the deep region near the river bend is a much narrower feature and controls the overall flow.

3.2.3. Vertical shear

There is minimal vertical shear in the stream-wise inflow velocities upstream of the turbine. As shown in Fig. 6, vertical variations are typically less than 10% of the mean flow value at the turbine hub height $z = -2$ m below the surface. As for lateral shear, results are the average from 338 stations lasting at least 10 minutes each, collected at positions immediately upstream of the turbine ($-20 < x < 0$ m). Vertical shear is assessed at three locations in cross-river dimension y , nominally turbine port ($y = -5$ m), turbine center ($y = 0$ m) and turbine starboard ($y = +5$ m). The pattern from these three profiles is consistent with the lateral shear result, in which flow is strongest at the starboard side of the turbine and in which spatial uncertainties exceed turbulent fluctuations.

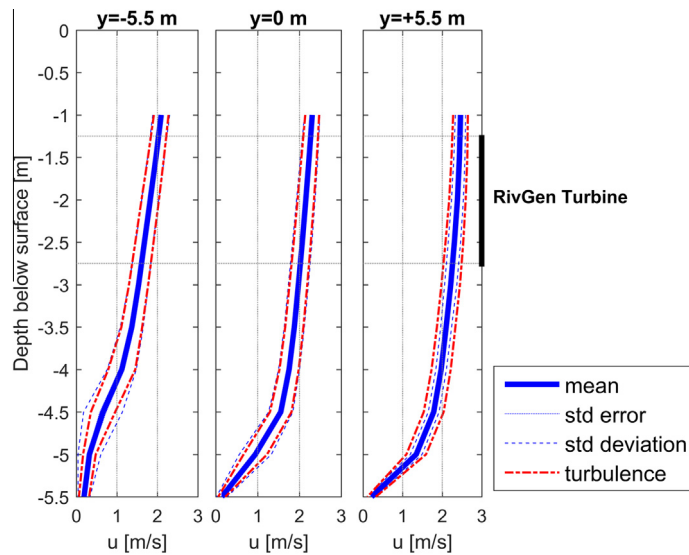


Fig. 6. Vertical shear shown as the stream-wise flow U versus depth below the surface at three positions in the cross-river direction: nominally turbine port ($y = -5.5$ m), turbine center ($y = 0$ m) and turbine starboard ($y = +5.5$ m). The blue dotted line is the standard error in determining the mean flow at each y . The blue dashed line is the standard deviation of individual stations. The red dashed line is variation expected from the measured turbulence intensity. The vertical extent of the RivGen turbine rotor sweep is shown as a black line ($2.75 < z < 1.25$ m).

3.2.4. Turbulence

The TKE spectra are most energetic at low frequencies, and show an expected $f^{-5/3}$ power law at high frequencies (Fig. 7). This is consistent with the isotropic cascade of energy from large scales to small scales through the inertial subrange. The vast majority of energetic fluctuations occur at low frequencies, $f < 0.2$ Hz.

The velocity distribution upstream of the turbine shows left-skewness and similar standard deviations and turbulence intensities at both measured locations. Table 1 shows statistics determined for 10-minute windows from two upstream locations taken at turbine hub height. Their locations are given relative to turbine center, with $+x$ downstream and $+y$ towards the starboard edge of the rotor. Though mean flow velocity varies with position, the turbulence characteristics are relatively consistent in this region of the river.

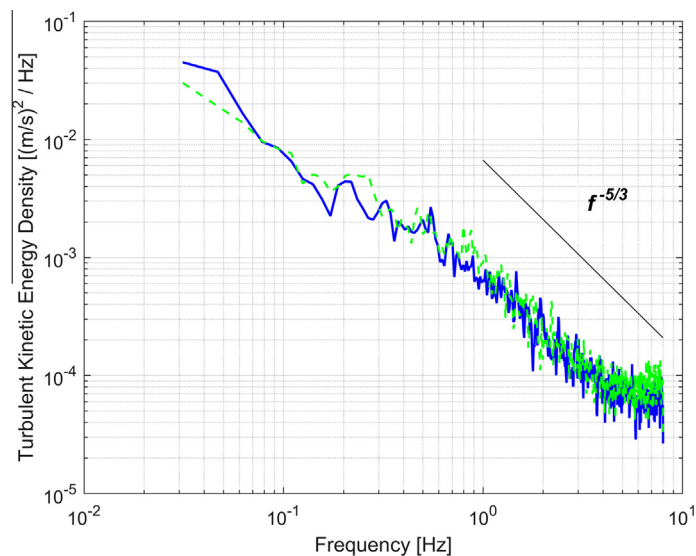


Fig. 7. Turbulent kinetic energy spectra density versus frequency from two different sets of upstream velocimeter data (10-minute windows each).

Table 1
Turbulence characteristics.

Location (m)	Mean velocity \bar{U} (m/s)	Standard Dev. σ (m/s)	Skewness G_1	Turbulence intensity (%)
[−62.5,8.2]	2.46	0.264	−0.186	10.7
[−48.2,−46.3]	2.40	0.228	−0.171	9.5

4. Turbine performance characterization

4.1. Measurement methodology

The turbine shore station included a resistive load bank with 15 discrete settings (nominally 2.3 Ω – 60 Ω). During performance testing, a shore operator maintained a specific setting for a period of several minutes, during which time the voltage and current across the load bank were recorded at 1 Hz. From voltage, turbine angular velocity was determined via $\omega = V/k$ where k is a known empirical coefficient that is specific to the generator. All data sets were time-stamped based on an internet-synchronized time server.

On three occasions, the turbine was stepped through sequential resistive loads for performance characterization (Table 2).

Results from the three trials are presented in Fig. 8 to demonstrate the magnitude of variability associated with different choices of inflow reference velocity (U_∞). In each case, a Dopocat positioned upstream of the turbine rotor provided an estimate for U_∞ . To develop these curves, quality-controlled velocity measurements were synchronized with turbine performance and instantaneous η and λ calculated using Eqs. (2) and (3), respectively. These instantaneous values were then averaged for each load setting. In retrospect, given the lateral shear present in the river (Section 3.2.2), the variability in the characteristic curves produced by point measurements is not unexpected.

4.2. Effects of turbulence

Fourier analysis of the generator power time-series generated from this testing shows that the generator responds predominantly to the low-frequency perturbations ($f < 0.2$ Hz) of the flow (Fig. 9). This time-series is a collection of 10-minute windows during which the resistive load setting was held at 5.4 Ω . A power spectra was determined using the same spectral analysis techniques as in Fig. 7 except that the velocity time-series (16 Hz) was down-sampled to 1 Hz for consistency with the generator power sampling rate and ensure equal spectral bandwidths. Due to the limited number of points, only adjacent frequency bands are merged to maintain resolution. Blade passage frequency is > 2.7 Hz and turbine rotation frequency is > 0.7 Hz so neither could be captured with this sampling rate. The resulting spectra are normalized by their variance and displayed on a common axis.

The turbine power output spectrum demonstrates that it responds most strongly to the energetic frequencies of the velocity spectra, which are $f < 0.2$ Hz. For a mean velocity of ~ 2 m/s, Taylor's hypothesis

$$f = l/\bar{U} \quad (8)$$

suggests that the turbine is sensitive to length scales l on the order of 10 m or greater. Because this is nearly the length of the rotor assembly, this implies that the turbine is primarily sensitive to “engulfing gusts”.

4.3. Invariant velocity hypothesis

As discussed in Section 3, the turbine hub-height mean velocity profile is relatively robust in time. If an assumption of time invariance is made, then the performance time series can be decoupled from the flow velocity time series. If valid, the characteristic performance curve for each of the three performance series collected during the point measurement attempts should be consistent.

Generally, the reference velocity across the turbine rotor is a function of both time and space as

$$U_\infty = U_\infty(x, y, z, t). \quad (9)$$

Table 2
Performance data collection periods.

Position	Date	Time (24 h, ADT)
A	8/22/2014	1021–1057
B	8/25/2014	1211–1234
C	8/25/2014	1235–1254

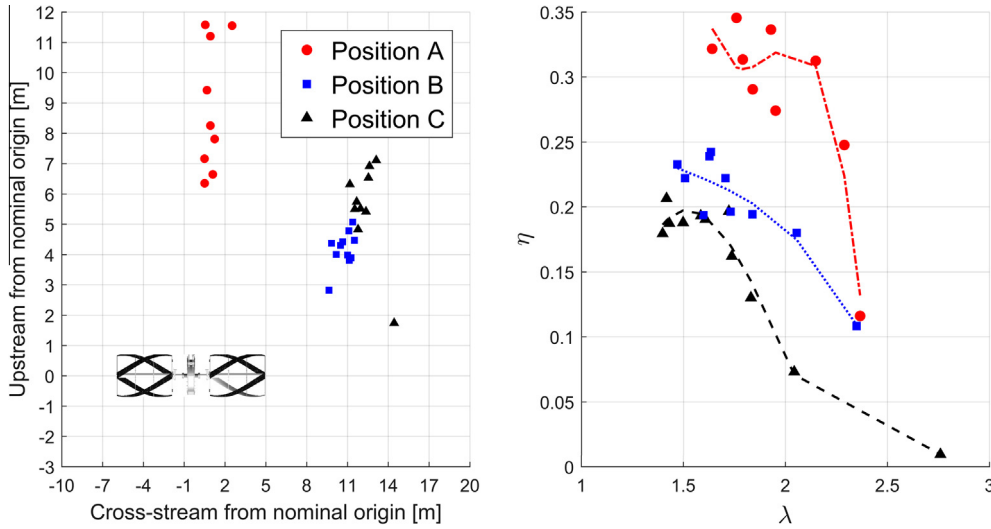


Fig. 8. Performance curves calculated from time-synchronized point measurements of velocity (right) and the locations at which they were measured relative to the nominal center of the coordinate system with turbine also shown (left). The color coding is consistent between plots.

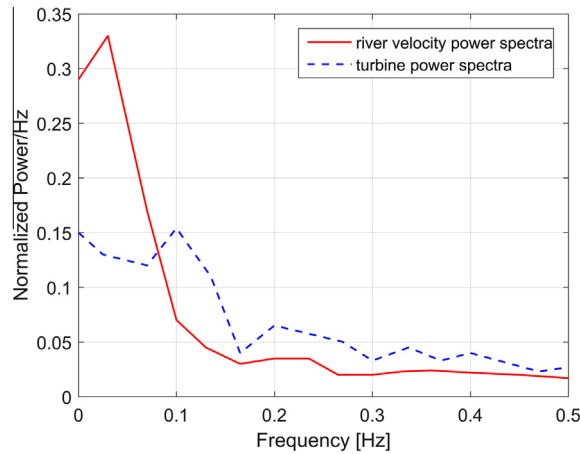


Fig. 9. Normalized power spectra density of generator power and turbulent kinetic energy.

Here, the infinity subscript denotes a reference inflow condition for turbine performance characterization, rather than the general velocity field described in Section 3. At a fixed position upstream of the turbine (constant x), the vertical shear is negligible (Section 3.2.3) and, if the lateral shear velocity profile is time-invariant (Section 3.2.1), a temporal average over a sufficiently long period approximates the lateral velocity profile across the turbine as

$$\langle U_\infty \rangle = \langle U_\infty(y, t) \rangle \tag{10}$$

where the angle brackets denote a temporal average. This corresponds to the mean velocity data presented in Fig. 5. To select a $\langle U_\infty \rangle$ representative of the flow across the entire turbine, the spatial average is calculated as

$$\overline{\langle U_\infty \rangle} = \overline{\langle U_\infty(y) \rangle} \tag{11}$$

where the overbar denotes a spatial average in the lateral direction, excluding the region occupied by the generator and drive shaft. From the time-averaged flow profile in Fig. 5, the span of points from end-to-end of the rotor were populated through linear interpolation at a resolution of 0.1 m and then averaged to obtain a single, representative value. The resulting profile is insensitive to this interpolation resolution provided it is fine enough to resolve the features of the flow (e.g. it is finer than the profile resolution).

From this temporally and spatially averaged free-stream velocity, an effective $\hat{\lambda}$ and $\hat{\eta}$ may be calculated as

$$\hat{\lambda} = \frac{\omega R}{\langle U_{\infty} \rangle} \quad (12)$$

$$\hat{\eta} = \frac{\langle IV \rangle}{\frac{1}{2} \rho \alpha \langle U_{\infty} \rangle^3 A} \quad (13)$$

The correction factor (α) is introduced because the cube of the temporal mean is not equal to the mean of the temporal cube. However, the instantaneous velocity cubed is not observable by Doppcat measurements due to the Doppler noise associated with 1 Hz sampling. An empirical correction factor is generated from 16 Hz velocimeter data (low noise sampling) as

$$\alpha = \frac{\langle U_{\infty}^3 \rangle}{\langle U_{\infty} \rangle^3}. \quad (14)$$

This yields $\alpha = 1.03$, which does not significantly change the results, but is included for completeness.

Alternatively, the discrepancy between the cube-of-means and mean-of-cubes could be addressed in a similar manner to wind-resource assessment over longer time scales. Fitting a Weibull distribution to velocimetry data, a correction factor α accounting for the discrepancy can be derived using the properties of the distribution [14], which also yields $\alpha = 1.03$.

4.4. Invariant velocity results

Performance characteristics obtained from Eqs. (12) and (13) during temporally-discontinuous measurements are presented as Fig. 10. The consistency of the curves suggests that the time-invariant assumption is valid over this time period. A third-order polynomial fit over the range $1.5 < \hat{\lambda} < 3$ is also shown and taken as representative of turbine performance in subsequent analysis. The differences between the performance at each load setting is likely the result of slight differences in mean stream velocity between the three data collection periods. For example, the highest $\hat{\eta}$ points for each case range from 0.25 to 0.27. This difference could be caused by a 1% difference (~ 0.02 m/s) in flow velocity. The relative insignificance of these differences supports the time-invariant hypothesis for the mean lateral inflow.

If the resulting performance curve is assumed to be valid at any position along the turbine rotor (that is $\hat{\eta}(\hat{\lambda}) = \eta_i(\lambda_i)$), then an analytical model can be constructed to evaluate local performance and the contribution of each segment of the rotor to aggregate power output. This model assumes a span-wise constant ω with spatially varying U_{∞} , resulting in local variations in λ_i that translate to local variations in η_i . For this model, the power curve is assumed symmetric about $\hat{\lambda} = 1.5$, so rotor sections operating locally $\lambda_i < 1.5$ generate power. However, if the average $\bar{\lambda}_i < 1.5$ across the rotor, the turbine is assumed to have stalled, generating no power (as was observed in the field). As for performance characterization, the turbine is approximated as a series of independent elements, $\Delta l = 0.1$ m. The power output is the summation of the relative contribution from each rotor element (i.e., $P = \Sigma P_i$).

Fig. 11 shows the aggregate power output from the turbine if performance is optimized at $\lambda_i = 1.59$, at a specific span-wise location. The maximum power output is 12.5 kW, in agreement with field observations. This does not provide additional certainty in the results (it is simply a different expression of turbine performance using the previous method). Overall, these results suggest that the location along the rotor where λ should be defined to maximize power generation is the one that maintains λ_i close to the global maxima for rotor elements in the most energetic flow, while keeping the average $\bar{\lambda}_i > 1.5$. This optimal location is a function of shear profile, shape of the performance curve, and rotor geometry.

This is illustrated by the pronounced discontinuity in power output if λ_i is “optimized” over the left-most rotor elements. The majority of the rotor is operating below $\lambda_i = 1.5$, and is stalled (below the minimum operable $\hat{\lambda}$ in Fig. 10). As the point defining $\lambda_i = 1.59$ moves farther right, the majority of the rotor begins to exceed $\lambda_i = 1.5$ and comes out of stall, producing power (in reality, the jump from a stalled rotor to near peak power would likely occur somewhat more gradually). Because the stall point is close to the $\hat{\lambda}$ for which $\hat{\eta}$ is maximized, (Fig. 10), once the rotor is no longer stalled, the sections in higher velocity are also at a near optimal λ_i , maximizing power output for the entire rotor, as shown in Fig. 12. As the defining point continues right, more of the rotor operates sub-optimally, slightly decreasing power output (Fig. 11).

The power contribution of a rotor element to the total power when the maximum power-generating governing point is selected is shown in Fig. 13. The highest contributing sections, as expected, fall within the high-velocity flow areas, though, less intuitively, the optimized point where $\lambda_i = 1.59$ does not.

5. Discussion

5.1. Resource assessment

The strong gradients in mean flow observed here are likely to be present at many other river turbine sites. This suggests that high-resolution site assessments prior to installation, precise placement during installation, and post-installation

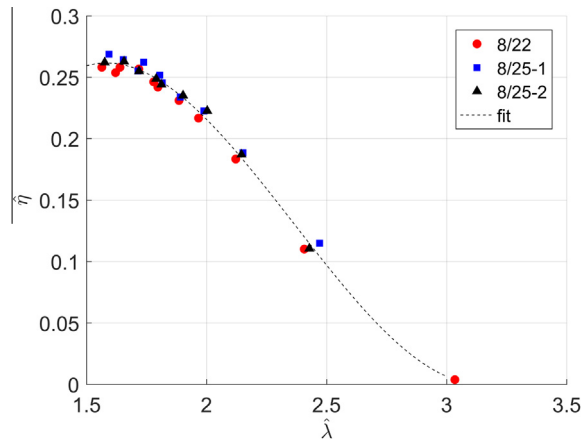


Fig. 10. Turbine performance assuming a temporally-invariant inflow, shown with 3rd-order fit. The clustering of the points is a result of the discrete load settings used for characterization.

surveys should be considered as best practices for commissioning river current turbines. The gradients also suggest that coarse numerical models are unlikely to accurately represent the velocity shear at river sites. Although the flow is turbulent, the time variations in the flow are minor in comparison with the spatial patterns. This is, in part, because the time variations are slow (> 5 s) and occur synoptically over scales that correspond to an “engulfing gust” for the turbine (> 10 m). The hybrid approach of mapping the flow with Doppler profilers and obtaining high-resolution turbulence data with Doppler velocimeters at a few locations is recommended.

5.2. Performance assessment

The maxima of the derived performance curve (Fig. 10) is substantially higher than maximum efficiency observed in pre-installation tow trials and computational modeling (27% vs. 19%). The disparity is also apparent if one were to assume $\hat{\eta}_{\max} = 19\%$ for the deployment in Igiugig, AK. A 12 kW power output would require an equivalent uniform velocity of 2.3 m/s, which is higher than inflow velocity measured across nearly all of the turbine at 5 diameters upstream (Fig. 5). Clearly, turbine performance is improved at this site relative to pre-installation tow trials. Blockage is not an entirely satisfactory hypothesis for this increase. As conventionally defined, the rotor swept area accounts for 3% of the river cross section. However, the rotor swept area accounts for 20% of the river depth. The free-surface deformation observed over the turbine suggests that vertical blockage or free surface proximity might affect performance or enable additional momentum transfer from the faster-flowing region of the river. Further investigation of this hypothesis requires information about inflow veloc-

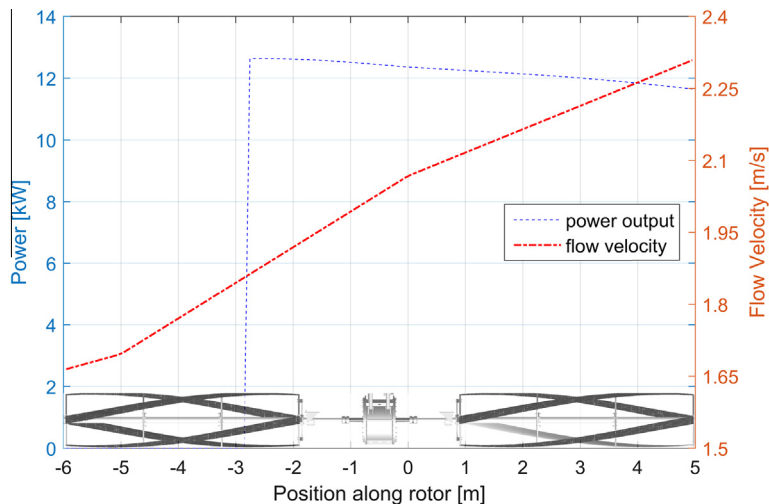


Fig. 11. Aggregate power output in sheared flow as function of point along the rotor where local performance is optimized. Also shown is the 2-D velocity profile (assumed time-invariant) at turbine hub depth. Turbine schematic superimposed for reference.

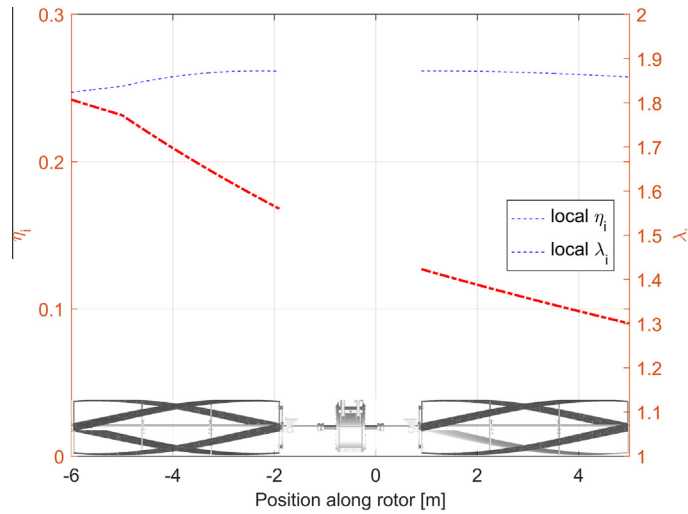


Fig. 12. Rotor element efficiency η_i shown with λ_i over the rotor for $\lambda_i = 1.59$ defined at $x = -2$. Note η_i is near its maximum in the highest energy flow regions.

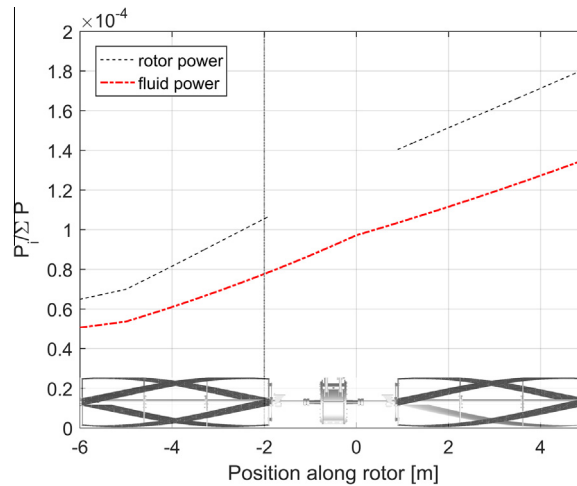


Fig. 13. Power generation and fluid power available as a fraction of the total over 0.1 m turbine sections for $\lambda_i = 1.59$ defined at $x = -2$ (vertical line).

ity on length scales equivalent to the turbine rotor both pre- and post-installation. Velocity surveys of this resolution carried out before and after turbine installation are recommended for robust performance assessments.

5.3. Turbine control in sheared flow

Laterally-sheared flow results in a spatially-varying λ and η along the turbine rotor. Control architectures that attempt to control either of these variables will need to define setpoints based on a specific location in the flow. For example, a linear proportional-integral controller on λ will require the correct combination of setpoint λ_s and definition location (i.e., location where $\lambda_s = \lambda_i$), as shown in Fig. 11. Non-ideal setpoints can be used without diminishing turbine performance, provided the velocity at the governing point results in an optimal λ_i for the portions of the rotor in the high-velocity flow. Because site conditions or turbine geometry may limit the allowable locations for a flow sensor, this technique could be used to implement an optimal control strategy. For example, if flow measurement was only possible in a lower velocity region, $\lambda_s = 2.0$ would result in optimal λ_i in the high-velocity region, maintaining a power output of 12.5 kW. Although the lateral shear profile observed at Igiugig appears to be synoptic on time scales of a week, a turbine deployed for longer periods might need to adjust to lower-frequency changes in the inflow. In the absence of any electromechanical changes to the turbine, a change in peak power output could indicate a change in shear profile or mean velocity magnitude. A periodic adjustment of λ_s could

be used to compensate using performance data alone to identify a new optimum set point (albeit at the cost of lost generation during this re-evaluation) following an extremum-seeking control algorithm [3,15].

In theory, a turbine could be deployed with adequate instrumentation to provide knowledge of its instantaneous inflow profile (i.e. an along-turbine array of upward looking Doppler profilers). If the turbine was characterized by the averaging method described above, the appropriate velocity to use for defining the ideal tip speed ratio would be the instantaneous spatial average, although it is likely this quantity would need to be averaged over several measurements to acquire a low-noise estimate.

6. Conclusion

Point measurements of inflow velocity cannot provide consistent power-performance curves when non-uniform velocities are present upstream of the rotor. At a specific site (Igiugig, AK (USA)), a limited number of point measurements provide temporally-resolved information about turbulence characteristics. These are combined with spatially-resolved mean flow measurements, shown to be robust over time-scales on the order of a week, to obtain a representative inflow velocity through spatial averaging. Spatially-averaged forms of the non-dimensional performance coefficients (tip-speed ratio and water-to-wire efficiency) are presented. Performance curves calculated from discrete observations of turbine power generation are consistent, suggesting that the temporal-spatial averaging method is reasonable. Velocity shear has implications for turbine control schemes. Defining a representative reference velocity will be a challenge for any control strategy that requires knowledge of free-stream velocity (e.g. tip-speed ratio control). A substantial performance variation is observed between these results and prior performance characterization in a uniform inflow. While several hypotheses for the cause of this discrepancy are possible, the underlying reason cannot be determined conclusively from available data. This result highlights how rigorous characterization of early turbine deployments can benefit resource and performance assessment methodologies.

Acknowledgments

This material is based upon work supported by the Department of Energy under DE-EE0006397. Support from Nortek USA, the Alaskan field crew (Joe Talbert, Alex deKlerk, Curtis Rusch, Ryan Tyler, and Monty Worthington), ILC camp, Dena'ina Air Taxi, and the village of Igiugig is gratefully acknowledged.

References

- [1] M.J. Khan, G. Bhuyan, M.T. Iqbal, J.E. Quaioco, Hydrokinetic energy conversion systems and assessment of horizontal and vertical axis turbines for river and tidal applications: a technology status review, *Appl. Energy* 86 (10) (October 2009) 1823–1835.
- [2] Tony Burton, Nick Jenkins, David Sharpe, Ervin Bossanyi, *Wind Energy Handbook*, Second ed., Wiley, Hoboken, NJ, 2011.
- [3] Tinglong Pan, Zhicheng Ji, Zhenhua Jiang, Maximum power point tracking of wind energy conversion systems based on sliding mode extremum seeking control, 2008 IEEE Energy 2030 Conf., 2008.
- [4] R.T. Cheng, J.W. Gartner, Complete velocity distribution in river cross-sections measured by acoustic instruments, in: *Proc. IEEE/OES Seventh Work. Conf. Curr. Meas. Technol.* 2003, 2003, pp. 21–26.
- [5] Ocean Renewable Power Company, *At Small River Sites: ORPC's RivGen Power System*, 2014.
- [6] Vincent Neary, Carlos Michelen, Andrew Murphy, Ryan Coe, Hal Youngren, Numerical modeling study to investigate RivGen strut drag on power performance. Technical Report Fig. 1, Sandia National Laboratories, Albuquerque, NM, 2014.
- [7] Peter Bachant, Martin Wosnik, Performance measurements of cylindrical- and spherical-helical cross-flow marine hydrokinetic turbines, with estimates of exergy efficiency, *Renew. Energy* 74 (2015) 318–325.
- [8] Jim Thomson, Levi Kilcher, Marshall Richmond, Joe Talbert, Alex DeKlerk, Brian Polagye, Maricarmen Guerra, Rodrigo Cienfuegos, Tidal turbulence spectra from a compliant mooring, in: *In Proc. 1st Mar. Energy Technol. Symp.*, Washington, D.C., 2013.
- [9] Levi F. Kilcher, Jim Thomson, Determining the spatial coherence of turbulence at mhk sites, in: *Proc. 2nd Mar. Energy Technol. Symp.*, Seattle, WA, 2014, pp. 1–7.
- [10] J. Thomson, B. Polagye, V. Durgesh, M.C. Richmond, Measurements of turbulence at two tidal energy sites in Puget sound, WA, *IEEE J. Ocean. Eng.* 37 (3) (July 2012) 363–374.
- [11] Elizabeth A. Nystrom, Kevin A. Oberg, Chris R. Rehmann, Measurement of turbulence with acoustic doppler current profilers - sources of error and laboratory results, *Hydraul. Meas. Exp. Methods* 2002 (2002) 1–10.
- [12] Yadolah Dodge, *The Concise Encyclopedia of Statistics*, vol. 38, Springer Science + Business Media, 2011.
- [13] TerraSond Ltd., Kvichak River RISEC Project Resource Reconnaissance & Physical Characterization Final Report. Technical report, TerraSond Ltd., Palmer, AK, 2011.
- [14] Y.K. Sanusi, S.G. Abisoye, Estimation of wind energy potential in southwestern Nigeria, *Pac. J. Sci. Technol.* 12 (2) (2011) 160–166.
- [15] C. Zhang, Raul Ordonez, Extremum-Seeking Control and Applications A Numerical Optimization-Based Approach, 18 ed., Springer, Hoboken, NJ, 2012.